Electrical & Computer Engineering Theses & Dissertations

Electrical & Computer Engineering

Spring 2011

Design and Demonstration of a Miniature Lidar System for Rover Applications

Benjamin Robinson
Old Dominion University

Follow this and additional works at: https://digitalcommons.odu.edu/ece_etds

Part of the Aerospace Engineering Commons, Atmospheric Sciences Commons, Computer Sciences Commons, Remote Sensing Commons, and the Robotics Commons

DESIGN AND DEMONSTRATION OF A MINIATURE LIDAR

SYSTEM FOR ROVER APPLICATIONS

by

Benjamin Robinson
B.S.E.E. May 2009, Old Dominion University

A Thesis Submitted to the Faculty of Old Dominion University in Partial
Fulfillment of the Requirements for the Degree of

MASTER OF SCIENCE

ELECTRICAL & COMPUTER ENGINEERING

OLD DOMINION UNIVERSITY
May 2011

Approved by:

Hani E. Elsáyed-Ali (Director)

Amin Dharamsi (Member)

M. Nurul Abedin (Member)

ABSTRACT

DESIGN AND DEMONSTRATION OF A MINIATURE LIDAR SYSTEM FOR ROVER APPLICATIONS

Benjamin Robinson
Old Dominion University, 2011
Director: Dr. Hani E. Elsayed-Ali

Public awareness of harmful human environmental effects such as global warming has increased greatly in recent years and researchers have increased their efforts in gaining more knowledge about the Earth's atmosphere. Natural and man-made processes pose threats to the environment and human life, so knowledge of all atmospheric processes is necessary. Ozone and aerosols are important factors in many atmospheric processes and active remote sensing techniques provide a way to analyze their quantity and distribution.

A compact ground-based lidar system for a robotic platform meant for atmospheric aerosol measurements was designed, tested, and evaluated. The system will eventually be deployed for ozone and aerosol measurements in Mars and lunar missions to improve our knowledge and understanding of atmospheres on Mars and the Moon. All of the major subsystems were described in detail and atmospheric testing was performed to test the operability of the receiver system to acquire the lidar return signal from clouds and aerosols. The measured backscattered results are discussed and compared with theoretical results.

This thesis is dedicated to my beautiful wife Keren, who encouraged me through the entire graduate school process, and to my loving grandmother Ruth, may she rest in peace.

ACKNOWLEDGEMENTS

I would like to thank my advisor, Dr. Hani Elsayed-Ali, for guiding me through my entire collegiate career and for providing me with the opportunity to pursue a master's degree. In addition, I would like to thank Dr. Nurul M. Abedin of NASA Langley Research Center for supporting my thesis research, spending countless hours in and out of the lab, and diligently helping me edit this thesis. I would also like to thank Dr. Amin Dharamsi for providing time and effort as a committee member on such short notice.

I would also like to thank all of the members of the MIDP program at NASA Langley Research Center. Each member has provided me with valuable insight and has helped me achieve my ultimate goal of completing this thesis research.

Additionally, I would like to thank the Virginia Space Grant Consortium for the scholarship that was provided. Without their assistance, I would not have been able to financially make it through graduate school.

Finally, I would like to thank my family for their unlimited support, especially my wife Keren. She picked up my spirit whenever I was down, and I could not have achieved success without her.

TABLE OF CONTENTS

LIST OF TABLES

LIST OF FIGURES

CHAPTER I

INTRODUCTION

Many research studies and reports have been published in recent years that seek to describe the negative effect that humans have on the environment. Whether it is global warming or ozone depletion, public awareness of such harmful environmental effects has increased greatly. With the influx of widespread atmospheric observations, researchers also have a greater knowledge and understanding of the Earth's atmosphere. Many natural and man-made processes pose threats to not only the environment but also human life. This makes it vitally important to improve our knowledge of any and all atmospheric processes. The quantity and distribution of ozone and aerosols are the most important factors for many atmospheric processes.

Ozone (O_3) is extremely important since stratospheric ozone protects us from harmful ultraviolet solar radiation. Although it is beneficial in the stratosphere, it is harmful in the troposphere because it acts as an air pollutant that damages human health and vegetation. This makes the buildup of ozone in the troposphere an important area of study for atmospheric researchers. Aerosols are minute suspensions of solid or liquid particles in air. They are ever-present in air and are often observable as dust, smoke, and haze. Aerosols directly affect the Earth's energy budget by scattering and absorbing radiation and indirectly affect it by modifying amounts and microphysical radiative properties of clouds.

The journal model used for this thesis is *Optical Engineering.*

To get a better understanding of aerosols, this chapter discusses them in more detail along with their atmospheric effects. Since lidar is an important active remote sensing technique for atmospheric aerosol measurements, lidar system architecture and theoretical analysis of the lidar equation are discussed in the following sections.

1.1 Aerosols

Since World War II, aerosols have been recognized as an important topic of applied science.[1] They play a significant role in the atmosphere and are involved in many atmospheric processes. On a global basis, aerosols derive predominantly from natural sources such as sea salt and dust. However, manmade aerosols, which come primarily from sources of combustion, can dominate highly populated or industrialized regions. Figure 1 shows an example of how dominant manmade aerosols have become a problem in Los Angeles.

The introduction of aerosols into the atmosphere alters the intensity of sunlight backscattered to space, absorbed in the atmosphere, and arriving at Earth's surface. This perturbation of sunlight by aerosols is called aerosol radiative forcing (RF).[2] On a global average, the sum of direct and indirect aerosol RF calculated at the top of the atmosphere is negative (cooling effect), which offsets some of the positive (warming) aerosol RF in the lower atmosphere caused by manmade greenhouse gases.[2] Due to spatial and temporal non-

uniformity of aerosol RF, the net effect is not equal and thus measuring and studying aerosols becomes an important scientific practice.
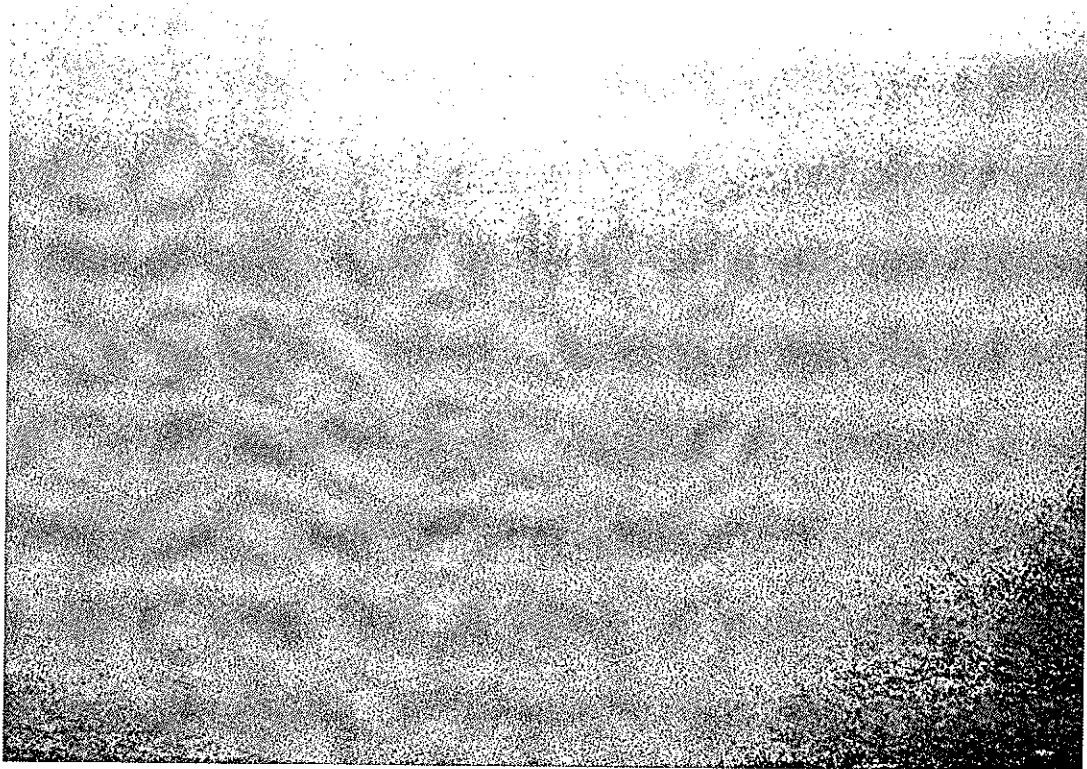
Figure 1: Los Angeles in the haze at sunset. Pollution aerosols scatter sunlight causing an intense orange-brown glow.[2]

1.1.1 Troposphere

The troposphere, starting from the Earth's surface and ending at approximately 10 km, is the lowest portion of the atmosphere. The troposphere can be divided into the planetary boundary layer, extending from the surface to approximately 1 km, and the free troposphere, extending from 1 km to 10 km.[1] Aerosols are typically a dominant component of the boundary layer, and they continue to increase as cities become more industrialized.

Aerosol residence times in the troposphere are about 1 to 2 weeks, meaning that anthropogenic aerosols would disappear from the planet in 2 weeks if all SO_2 sources were shut off today.[1] On the other hand, greenhouse gases last for decades to centuries, but they take much longer to be fully transformed into equilibrium climate warming because of the great inertia of the climate system. As a result, if both CO_2 and aerosol emissions were to cease today, the Earth would continue to warm as the climate system continues to respond to the accumulated amount of CO_2 already in the atmosphere.[1] In any case, the measurement of aerosols, especially in the troposphere, is important to atmospheric researchers since it provides information about their quantity and distribution.

1.2 Atmospheric Aerosol Measurement Approaches

A variety of available techniques are capable of obtaining valuable information about aerosols. The primary approach used today involves active remote sensing, in which radiation is used to interact with various molecules and aerosols to obtain information such as quantity, size, or distribution of the particles. Satellite remote sensing allows measurement-based characterization of aerosols on a global scale.[2]

In remote sensing, radiation is produced by the transmitter and emitted in the form of light, radio waves, microwaves, or acoustic waves. The emitted

radiation is backscattered by the atmospheric constituents and collected with a receiver system that includes a telescope, optics, and detectors. The collected light is then analyzed. This type of sensing has the advantage of being independent of time of day and natural radiation sources. Lidar, which has been deployed on various platforms and missions, is an example of an active remote sensing system, and it has the advantage of displaying high vertical resolution profiles at various altitudes.[3]

1.3 Lidar System Architecture

Lidar, which stands for light detection and ranging, is an active remote-sensing technology that measures the properties of scattered light with respect to the distance or range of a target. Lidar systems are based upon the same principles that are used in radar and sonar systems. A radar system uses radio waves for detection and ranging, but a lidar system has the distinct advantage of using light for detection and ranging. Lidar is much better for certain applications because very small particles, such as aerosols, can be easily detected due to the fact that a lidar uses much shorter wavelengths in the electromagnetic spectrum. Radar systems use radio waves that may not detect small particles because the wavelength of radio waves is too large for accurate detection of small particles.[4]

The operation of a lidar system is fairly simple. A light pulse is transmitted into the atmosphere, and that light is scattered in all directions by various

atmospheric constituents such as molecules, atoms, aerosols, clouds, or dust particles. Some of the scattered light is reflected back to the lidar system, where it is focused by a telescope into a photodetector. The photodetector usually is connected to a data acquisition system and a computer that can measure the amount of backscattered light as a function of distance. From that description, it is clear that any basic lidar system will require four main components: a laser, a telescope assembly, a photodetector (APD or PMT), and a computer system for data acquisition.[5] A typical lidar system block diagram can be seen below in Figure 2.
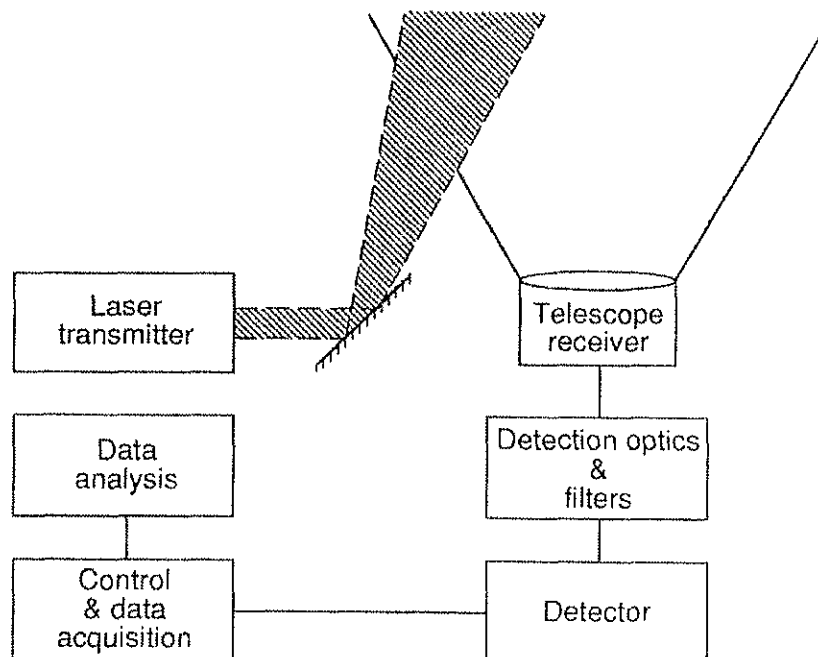
Figure 2: Typical lidar system block diagram.

Lidar systems can be arranged in two basic configurations: mono-static or bi-static. In bi-static configurations, the laser (transmitter) is separated from the

receiver by a relatively large distance, and both are typically set at different angles to achieve certain spatial resolution. In mono-static configurations, the laser and receiver are set up in the same location. This type of configuration is the most common, and it can be set up in two different arrangements: bi-axial or co-axial. For bi-axial arrangements, the axes of the laser and telescope are parallel, but they are offset by some distance so that the laser enters the field of view of the telescope at a specific range. For co-axial arrangements, the laser beam is steered towards the front of the telescope, where it exits parallel to the telescope in the middle of the telescope's central obstruction.[5] The lidar system used for this thesis has a mono-static co-axial arrangement. Figure 3 illustrates a bi-axial and co-axial lidar arrangement.
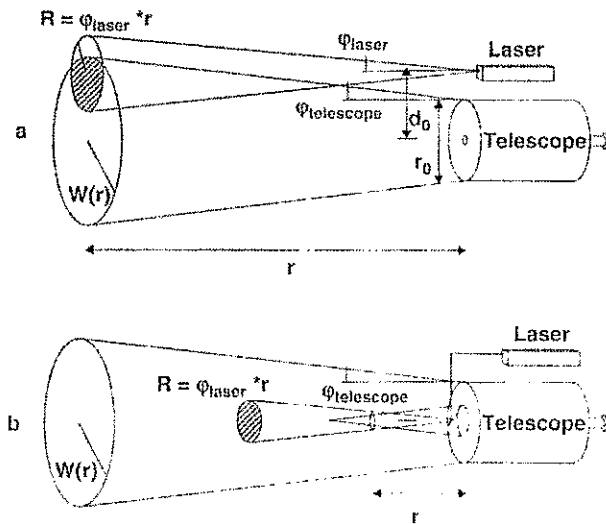
Figure 3: a) Bi-axial lidar arrangement. b) Co-axial lidar arrangement.[5]

1.4 Theoretical Analysis of the Lidar Equation

The lidar equation, which can appear in many different forms depending on the particular lidar system or application, is the basic equation in the field of laser remote sensing that describes the relationship between the received power of a lidar receiver channel and distance or range. As laser light propagates through the atmosphere, some photons are backscattered from various atmospheric particles, and the lidar equation makes two assumptions about this scattering process: scattering processes are independent and only single scattering occurs.[6] In atmospheric scattering, air particles are separated adequately due to low atmospheric density, meaning they undergo random motion and the contributions to the total scattered energy by the numerous particles have no phase relations. This assumption allows the total intensity to be calculated by simply adding the intensity of each independent individual particle. Single scattering means that a particle is only scattered once. Multiple scattering is excluded because the probability for such scattering is negligible.

Whenever light strikes a medium, it is scattered and/or absorbed. Light scattered in the atmosphere is grouped into two general types of scattering: elastic scattering and inelastic scattering.[7] In elastic scattering, the wavelengths of the scattered light are the same as the wavelengths of the incident laser light. Mie and Rayleigh scattering are two common examples of elastic scattering. For inelastic scattering, the wavelength of the scattered light is not equal to the wavelength of the incident laser light. Excitation of the energy levels in the

scattering molecules causes the shift in wavelength. Raman scattering is the most common form of inelastic scattering. Figure 4 displays a proper physical interpretation of the different types of atmosphere absorption and scattering. Only elastic scattering will be considered in this research thesis.
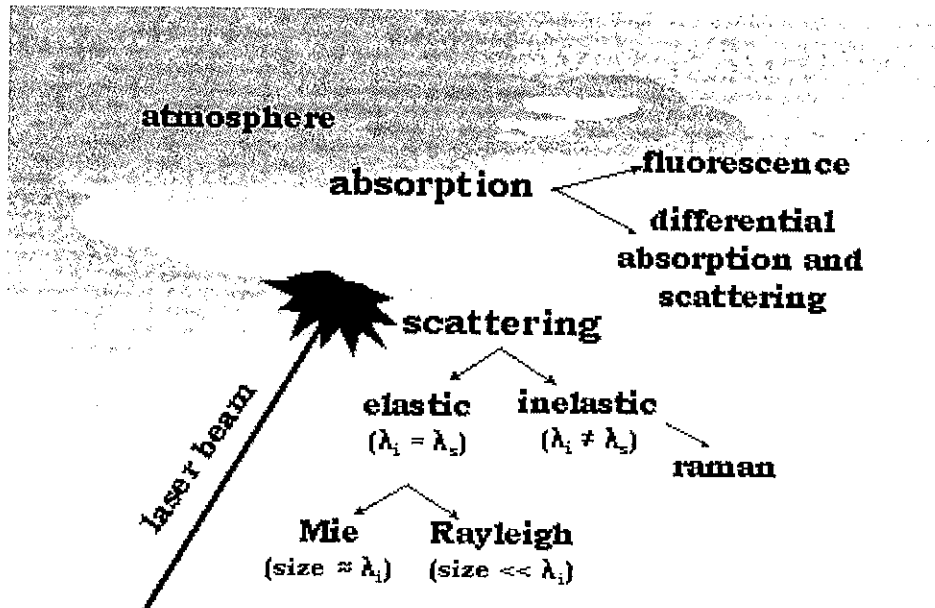
Figure 4: Types of atmospheric scattering and absorption.[7]

The most common and simplest form of the lidar equation is given as[8]

$$P(R) = \frac{C\beta(R)T^2(R)}{R^2}$$

(1)

where

$P(R)$ Received power

C Lidar constant (different for each lidar system)

$\beta(R)$ Volume backscattering coefficient at range R

$T^2(R)$ Two-way transmittance (to atmosphere and back) to range R

R Range.

This basic form can be further expanded so that the single-scattering elastic form of the lidar equation is described as[9]

$$P(R) = P_0\beta(R)\frac{c\tau}{2}\frac{A}{R^2}\eta O(R)T^2(R) \qquad (2)$$

where

$P(R)$ Instantaneous received power

P_0 Transmitted power at time t_0

$\beta(R)$ Volume backscattering coefficient at range R

$\dfrac{c\tau}{2}$ Effective spatial pulse length

$\dfrac{A}{R^2}$ Probability that a backscattered photon is collected by the telescope where A is the telescope area and R is range

η Overall optical efficiency of receiver and detector

$O(R)$ Overlap function of laser beam and telescope's FOV

$T^2(R)$ Two-way transmittance (to atmosphere and back) to range R.

The terms $P(R)$ and $P_0(R)$ represent the power received from a distance

and the average power of a single laser pulse, respectively. Some lidar equations

will represent the power in terms of photons, but this thesis research is interested

in power, which can be determined by the energy of the laser pulse E_{Pulse} divided

by the pulse width t_{Pulse}.

$$P_0 = \frac{E_{Pulse}}{t_{Pulse}}$$
(3)

The backscatter coefficient $\beta(R)$, which expresses the amount of

backscattered light towards the receiver, is an atmospheric parameter that

primarily determines the strength of the return lidar signal.[10] For this lidar

application, the backscatter coefficient is the value of the scattering coefficient for

the scattering angle of 180°. Knowing this value, the backscatter coefficient

results in the sum of all backscatters and can be written as[10]

$$\beta(R) = \sum_j N_j(R) \frac{d\sigma_{j,scatter}}{d\Omega}(\pi)$$
.(4)

The term $N_j(R)$ is the concentration of scattering particles of kind j in the

volume that is illuminated by the laser pulse. The term $d\sigma_{j,scatter}(\pi)/d\Omega$ is the

differential scattering cross section for the backward direction of the particle at an

angle π.

Laser light is scattered by air molecules and aerosols (particles) in the

atmosphere[11], so it is often useful to write the backscatter coefficient as[10]

$$\beta(R) = \beta_{mol}(R) + \beta_{aer}(R) \tag{5}$$

Molecular scattering $\beta_{mol}(R)$ largely depends on air density and will

decrease with height if the observation is made from the ground.[10] Aerosol

scattering $\beta_{aer}(R)$ is highly variable on all temporal and spatial scales since

aerosols represent such a vast number of different scatterers that vary in

amount.[10]
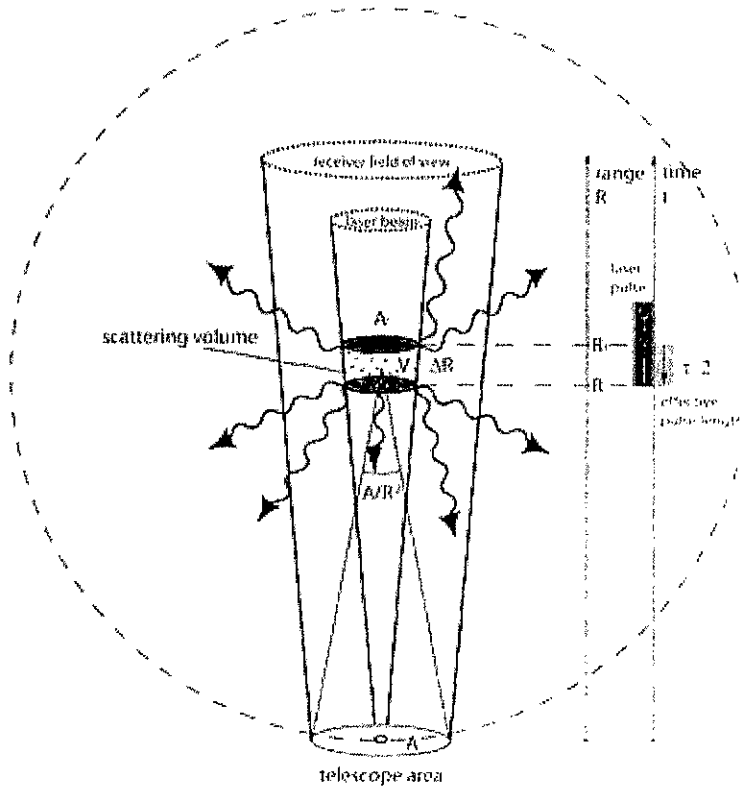
Figure 5: Illustration of lidar geometry.[11]

To determine the illuminated scattering volume, the range R must be calculated. When a lidar signal is detected at time t after the leading edge of the laser pulse was emitted, the backscattered light traveled the distance $R_1 = ct/2$. At the same time, backscattered light from the trailing edge of the laser pulse travels the distance $R_2 = c(t-\tau)/2$. Therefore, $\Delta R = R_2 - R_1 = c\tau/2$ gives the effective spatial pulse length, which is also commonly called the lidar signal range resolution.[10] As shown in Figure 5, the effective spatial pulse width can be determined from the time delay in sending, receiving, and processing the laser light.[11] By using the length of the laser pulse τ_L, but ignoring the negligible reaction time of the interaction of laser light with particles τ_W and the time constant of the detecting electronics τ_N, the lidar signal range resolution is given as[11]

$$\Delta R = \frac{c\tau}{2} = \frac{c(\tau_L + \tau_N + \tau_W)}{2} = \frac{c\tau_L}{2} \qquad .(6)$$

The term A/R^2 represents the probability that a backscattered photon is collected by the telescope, where A is the area of the telescope and R is the distance or range.

The term η represents the optical efficiency of the lidar transmitter and receiver, and $O(R)$ is the laser-beam receiver-field-of-view overlap function. The overlap function will equal one when the laser-beam is completely within the field-of-view of the telescope.[10]

The term $T^2(R)$ is the transmission term, and it describes the part of light that gets lost on the way from the lidar to the scattering volume. The factor 2 represents the light traveling to and from the scattering volume. The term is derived from the Lambert-Beer-Bouguer law for lidar and can be written as[11]

$$T^2(R) = \exp\left[-2\int_0^R \alpha(R')dR'\right] \tag{7}$$

The term $\alpha(R)$ represents the extinction coefficient. It is computed similarly to the backscatter coefficient as the product of concentration and extinction cross section $\sigma_{j,ext}$ for every type of scatterer j and is written as[10]

$$\alpha(R) = \sum_j N_j(R)\sigma_{j,ext} \tag{8}$$

Extinction results from absorption and scattering of light by both molecules and aerosols (particles)[10], so it is often given as the sum of all four components, or[10]

$$\alpha(R) = \alpha_{mol,sca}(R) + \alpha_{mol,abs}(R) + \alpha_{aer,sca}(R) + \alpha_{aer,abs}(R) \tag{9}$$

The term $\alpha_{mol,sca}(R)$ represents the extinction from molecular scattering, $\alpha_{mol,abs}(R)$ represents the extinction from molecular absorption, $\alpha_{aer,sca}(R)$ represents the extinction from aerosol scattering, and $\alpha_{aer,abs}(R)$ represents the

extinction from aerosol absorption. For this thesis, the absorption coefficients will be ignored to allow for easier calculations. The equation then becomes[10]

$$\alpha(R) = \alpha_{mol,sca}(R) + \alpha_{aer,sca}(R) = \alpha_{mol}(R) + \alpha_{aer}(R) \tag{10}$$

By consolidating all of the information described previously, a more general from of the lidar equation can be shown as

$$P(R) = P_0 \left[\beta_{aer}(R) + \beta_{mol}(R)\right]\frac{c\tau}{2}\frac{A}{R^2}\eta O(R)\exp\left\{-2\int_0^R \left[\alpha_{aer}(R') + \alpha_{mol}(R')\right]dR'\right\}. \tag{11}$$

1.5 Research Objective

As discussed in previous sections, active remote sensing instruments continue to be essential for many NASA missions. Planetary applications of such instruments would enable the much needed measurements of Martian wind and dust density profiles. As budgets decrease and technological growth accelerates, rovers continue to grow in popularity due to not only their remote access capabilities but also the option of sending a robot to perform tasks instead of a human being. Due to the factors above, this thesis focuses on developing a compact lidar receiver system to be used on a ground based rover for the detection of aerosols and cloud distributions. After further development and improvements, this system will eventually be deployed on Martian missions to assist in increasing our knowledge of the Martian atmosphere.

CHAPTER II

EXPERIMENTAL SETUP

This chapter describes the hardware configuration of the rover lidar system as shown in Figure 6. The actual rover system consists of numerous components for both raman spectroscopy and lidar as shown in Figure 7. Figure 8 shows the rover subsystem components necessary for lidar, which consists of the following: the laser (transmitter), the telescope assembly, the receiving optics (including components such as mirrors, filters, etc.), the photomultiplier tube (PMT), the power distribution unit (PDU), and the data acquisition system. Each of these subsystems will be discussed in detail.
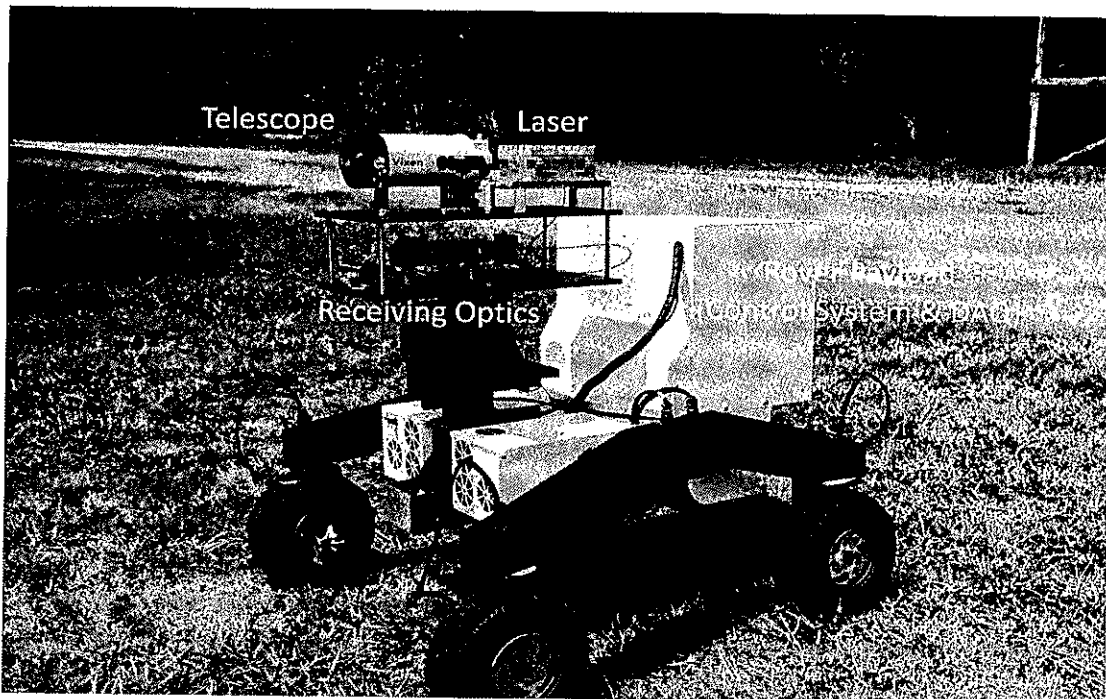
Figure 6: A picture of the rover lidar system outside with the major components labeled.
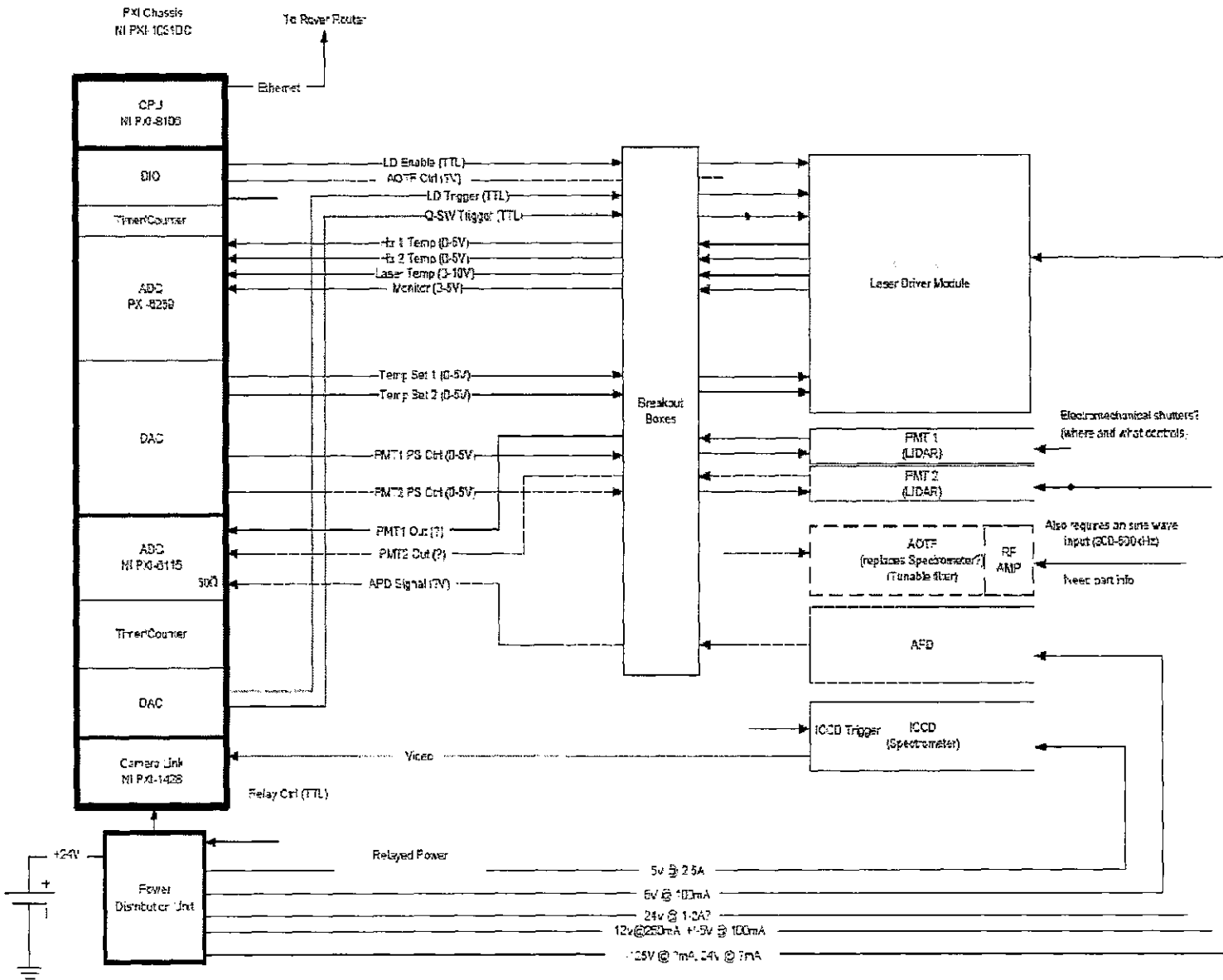
Figure 7: Combined (Raman and Lidar) rover system design.
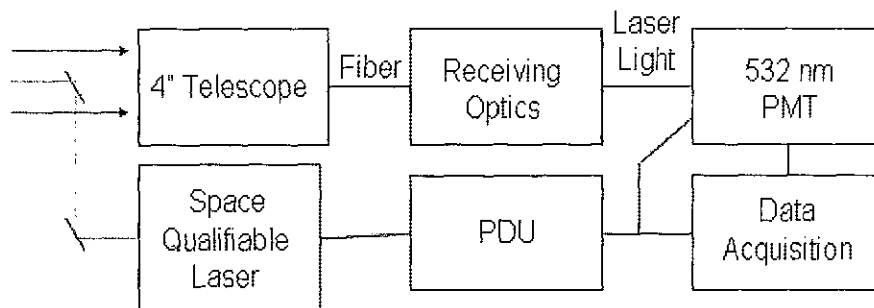
Figure 8: Miniature lidar rover system block diagram.

2.1 Lidar Transmitter

The main components of the lidar transmitter system are discussed in this section. The lidar transmitter consists of an all solid-state diode pumped Q-switched Nd:YAG laser mounted on the mast on the front of the rover, along with all of the associated power and lidar control units which are supported in the rover's rear payload. An optical schematic of the laser transmitter is shown in Figure 9.

Optical Schematic

1. Odd bounce Nd:YAG slab
2. Non-imaging telescope
3. Cr⁴⁺:YAG passive q-switch
4. Type I LBO doubler
5. Type II LBO tripler
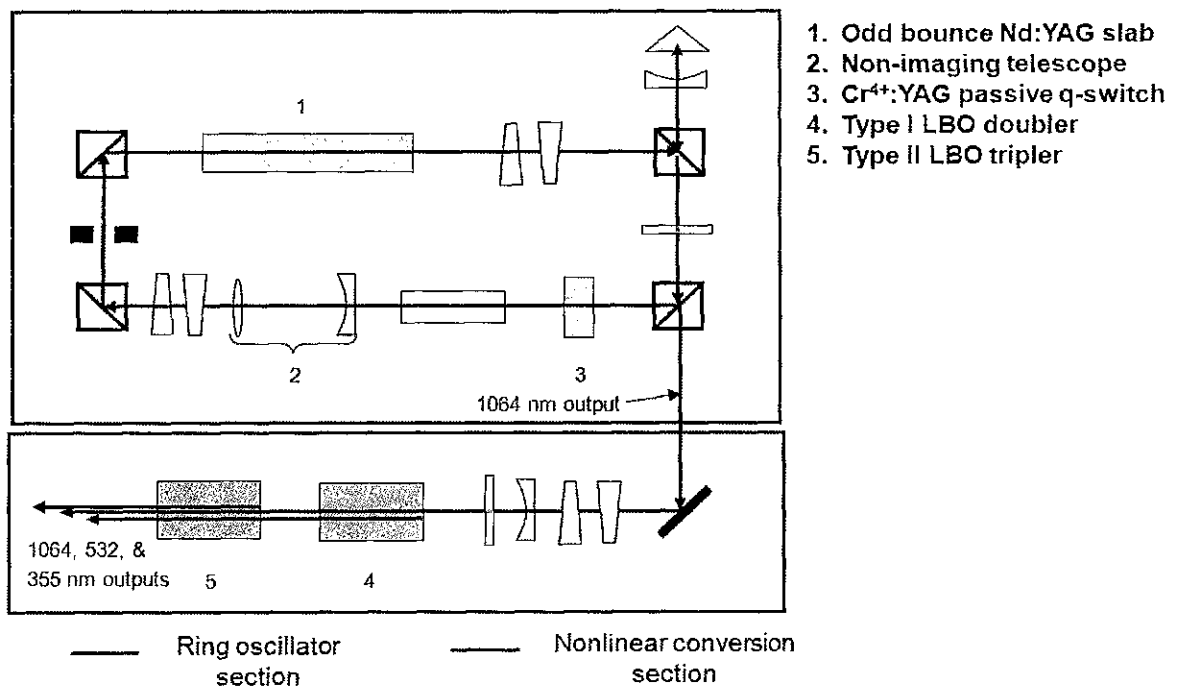
Figure 9: An optical schematic of the laser transmitter.[12]

2.1.1 Nd:YAG Laser Rod

The main component of the laser transmitter is the Nd:YAG

(Nd^{3+}:$Y_3Al_5O_{12}$) crystal slab, which can produce intra-cavity second harmonic

(532 nm) and third harmonic (355 nm) generation when combined with the Type I

LBO doubler and Type II LBO tripler. The yttrium ions in YAG (yttrium aluminum

garnet) can be replaced with rare earth laser-active ions such as neodymium

without strongly affecting the lattice structure, thus making Nd:YAG a popular

choice for laser crystals. Due to the approximately 3% difference in size between

the neodymium and yttrium ions, the amount of neodymium dopant must be

limited to approximately 1%. If more than 1% is used, then the crystal becomes severely strained.[13]

Nd:YAG is a four-level gain medium that offers excellent laser gain even for moderate excitation levels and pump intensities.[14] The gain bandwidth is small, but this allows for a high gain efficiency and low threshold pump power, which helps meet the rover's power requirements since the entire rover system runs on only two 12 VDC serially connected batteries. The crystal is diode pumped using a zigzag slab so that a robust and efficient optical design could be used to make the laser space-qualifiable. Diode pumping results in minimal heat generation which allows smaller electrical and cooling utility requirements. Also, the slab is mounted directly to the laser canister to allow conductive cooling of the laser head.

2.1.2 Q-Switching

The Nd:YAG laser utilizes a Cr^{4+}:YAG crystal to achieve passive Q-switching and produce a pulsed laser output at a repetition rate of 20 Hz. Passive Q-switching is an alternative technique to active Q-switching, where an acousto-optic modulator is incorporated into the laser resonator and acts as a shutter by blocking and unblocking the laser beam. In passive Q-switching, the acousto-optic modulator is replaced with a saturable absorber. The saturable absorber (Cr^{4+}:YAG crystal) initially introduces a high optical loss. Once the gain reaches this loss level and the pulse begins to build up, the absorber is saturated. This

means that the optical loss is reduced and the pulse buildup is accelerated. A short pulse is emitted shortly after the laser gain exceeds the resonator losses. After the pulse, the absorber returns to its high loss state before the gain recovers so that the next pulse is delayed until the gain medium's energy is replenished. Compared to active Q-switching, passive Q-switching is a simple and cost effective method to produce a pulsed output beam.

2.1.3 Intra-Cavity Frequency Doubling and Tripling

The Nd:YAG laser features intra-cavity second harmonic generation and third harmonic generation. The laser is split into a ring oscillator section and a nonlinear conversion section. The fundamental wavelength (1064 nm) that is generated in the ring oscillator section is passed to the nonlinear conversion section where second and third harmonic generations are performed by a Type I LBO doubler and a Type II LBO tripler. After passing through the two non-linear crystals, wavelengths of 1064 nm, 532 nm, and 355 nm are sent out as laser pulses.

Type I and Type II phase matching are two typical phase matching techniques that exploit birefringence to cancel phase mismatch. In Type I phase matching, the two fundamental beams have the same polarization in sum frequency generation, which is perpendicular to that of the sum frequency wave. In Type II phase matching, the two fundamental beams have different

polarization directions. This second type of phase matching is appropriate when the birefringence is relatively strong or the phase velocity mismatch is small.

The non-linear crystal that is used for second harmonic generation is a relatively low cost Type I LiB_3O_5 (LBO) crystal that provides high damage threshold and linearly polarized residual 1064 nm. The crystal also has high nonlinearity, a large acceptance angle, and low walk-off, thus making it very suitable for harmonic generation of laser radiation. A Type II LBO crystal is used for third harmonic generation. This crystal is anti-reflection coated for 1064 nm, 532 nm, and 355 nm. LBO triplers have been tested and achieved approximately 50% conversion efficiency from 1064 nm to 355 nm. In order to achieve the required temperatures for non-critical phase matching, the two LBO crystals are mounted in temperature controlled ovens. Temperature tuning of the ovens is used for the final fine tuning of both the second and third harmonic generation efficiencies to achieve the desired energies at each wavelength. The Type I LBO doubler temperature is maintained at 128.93 ± 1 degrees Fahrenheit, and the Type II LBO tripler temperature is maintained at 133.18 ± 1 degrees Fahrenheit.

2.1.4 Transmitter Optics

The output beam of the Nd:YAG laser, which consists of three separate wavelengths (355 nm, 532 nm, and 1064 nm), is directed towards a beam expander to reduce beam divergence. The 5x beam expander is designed to

keep the transmitted beam to a diameter of approximately 20 mm with a beam divergence of <0.5 mrad. The expanded beam is then directed towards a moveable mirror, which can be adjusted to direct the laser beam towards a second fixed mirror that is attached directly to a spider cage on the front of the telescope. Since the telescope and second beam-steering mirror are stationary, it is vital to adjust the first beam-steering mirror so that the axes of the beam and telescope are parallel with one another.

2.2 Receiver System

The lidar receiver system consists of a Vixen VMC110L Telescope, along with various receiving optics discussed in the next section. The telescope has a 110 mm primary mirror diameter with an F number of F/9.4 and a focal length of 1035 mm. An optical schematic of the telescope assembly and transmitter optics is shown in Figure 10. The telescope is connected to the receiving optics assembly by a 1-mm Polymicro Technologies fiber optic cable with a numerical aperture of 0.22 that transmits the received signal from the telescope to the receiver assembly, which houses the PMT and beam dumps.
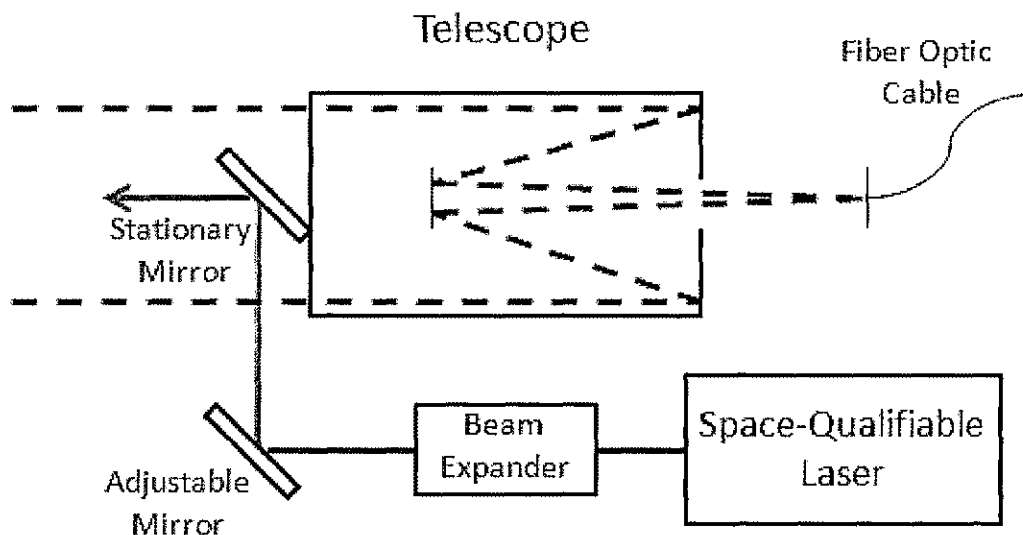
Figure 10: Optical schematic of telescope assembly and transmitter optics.

2.2.1 Receiving Optics

An optics plate mounted on the rover contains all of the receiving optics

used to detect atmospheric return signals. A simple optical schematic of the

receiving optics is shown in Figure 11. The PMT that is being used to measure

the 532 nm return signal was based on a circuit designed by Don Silbert (GFSC)

and modified by Terry Mack (Lockheed Martin). This design supports the

Hamamatsu R7400 metal package photomultiplier series tube. By using a small

telescope as a receiver, the lidar return signal will be very weak, so we need an

extremely sensitive PMT with low noise and high gain. This makes the

Hamamatsu PMTs an ideal choice for detectors since they have low noise, high

gain, and excellent response times, making them perfect for any light detection

application. The PMT requires voltages of 15 V and +/- 5 V for power, and it receives the power signals from the power distribution unit.

The output of the 1 mm fiber optic cable immediately passes through a collimating lens. Next, the beam passes through a notch filter that effectively splits the 355 nm beam from the rest of the signal and sends it to a beam dump. The signal then passes through another notch filter that splits the 532 nm beam from the rest of the signal. The 532 nm beam passes through a focusing lens and a narrowband pass filter before reaching the PMT. Next, the signal passes through a third notch filter that splits the 1064 nm beam from the rest of the signal. The 1064 nm is sent to a beam dump, and the rest of the signal is focused into a 100 µm fiber optic cable by a focusing lens. The other end of the cable is connected to a Raman spectrometer, which is not part of this thesis.
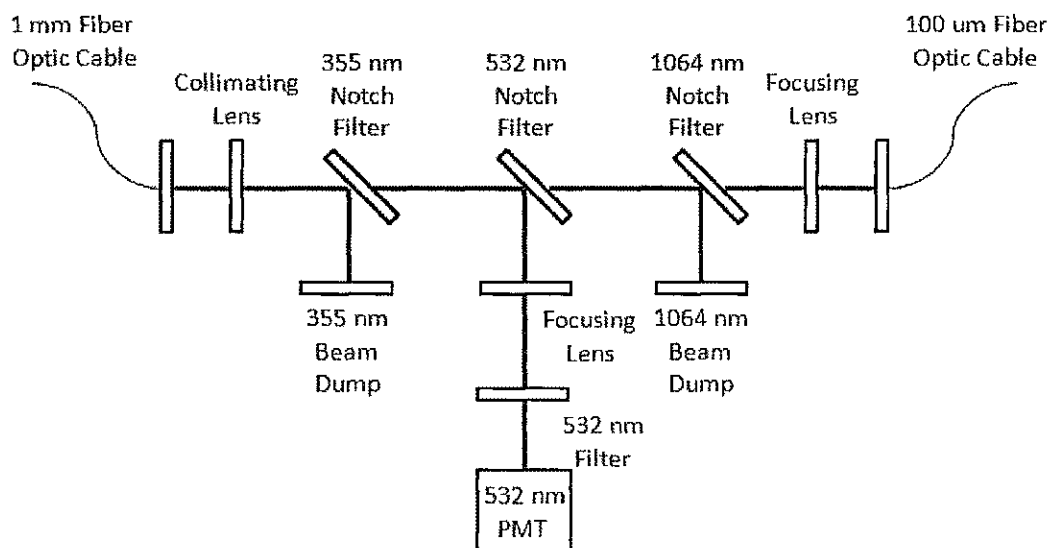
Figure 11: Optical schematic of receiving optics.

2.3 Power Distribution Unit

The power distribution unit (PDU) is the most vital part of not only the lidar system but the entire rover system. The PDU receives power from 2 12 V DC batteries connected serially (24 V DC total) and distributes it appropriately to the data acquisition system (NI PXI Chassis), the laser driver module, and the 532 nm PMT. The 24 V DC supply power is split and routed through EMI filters, relays, DC-DC convertors, and current sensing modules before being distributed to individual system components. It also routes control signals from the NI PXI Chassis to individual system components. The custom-built PCB board and the case to house it were populated so that jacks and connectors could be used to route signals to the appropriate system components.

2.4 Data Acquisition System

The data acquisition system consists of a NI PXI chassis (NI PXI-1031DC) that uses four cards: a NI PXI-8106 Embedded Controller, a NI PXI-6115 Multifunction I/O card for input and output signals, a NI PXI-6259 Multifunction DAQ card for input and output signals, and a NI PXI-1428 Image Acquisition card for the ICCD camera (for a separate Raman spectrometry application being used on the rover). The NI PXI-6115 card performs high-speed, analog data acquisition for the 532 nm atmospheric return signal and has 12 bit resolution along with a 10 MS/s sample rate. The card acquires 50 ms of data (each

individual laser shot), processes the data, and saves it in a text file. Each

individual shot is saved in a separate text file, but the LabVIEW program that

controls all of the signals contains an option to save any number of averaged

shots to reduce the amount of data. The data acquisition system runs from a

master LabVIEW program that controls input/output signals, control signals,

power signals, and steering on the rover.

2.5 Lidar and Rover Control

The rover system requires assorted components for lidar and rover

control. All of the components necessary for control are located on the rear

payload of the rover. The main component for control is the NI PXI chassis,

which handles lidar control and data acquisition. The PXI has been set up with a

router so that it can be remotely accessed from a laptop computer. The entire

rover system can be controlled from this remote connection. One LabVIEW

program controls rover movement and allows the user to control the movement

of the rover and the mast (for lidar or raman mode of operation) with a USB

joystick. Another LabVIEW program, which is shown in Figure 12, controls the

power relays, I/O signals, and lidar experimental values.

Figure 12: LabVIEW Control Panel.
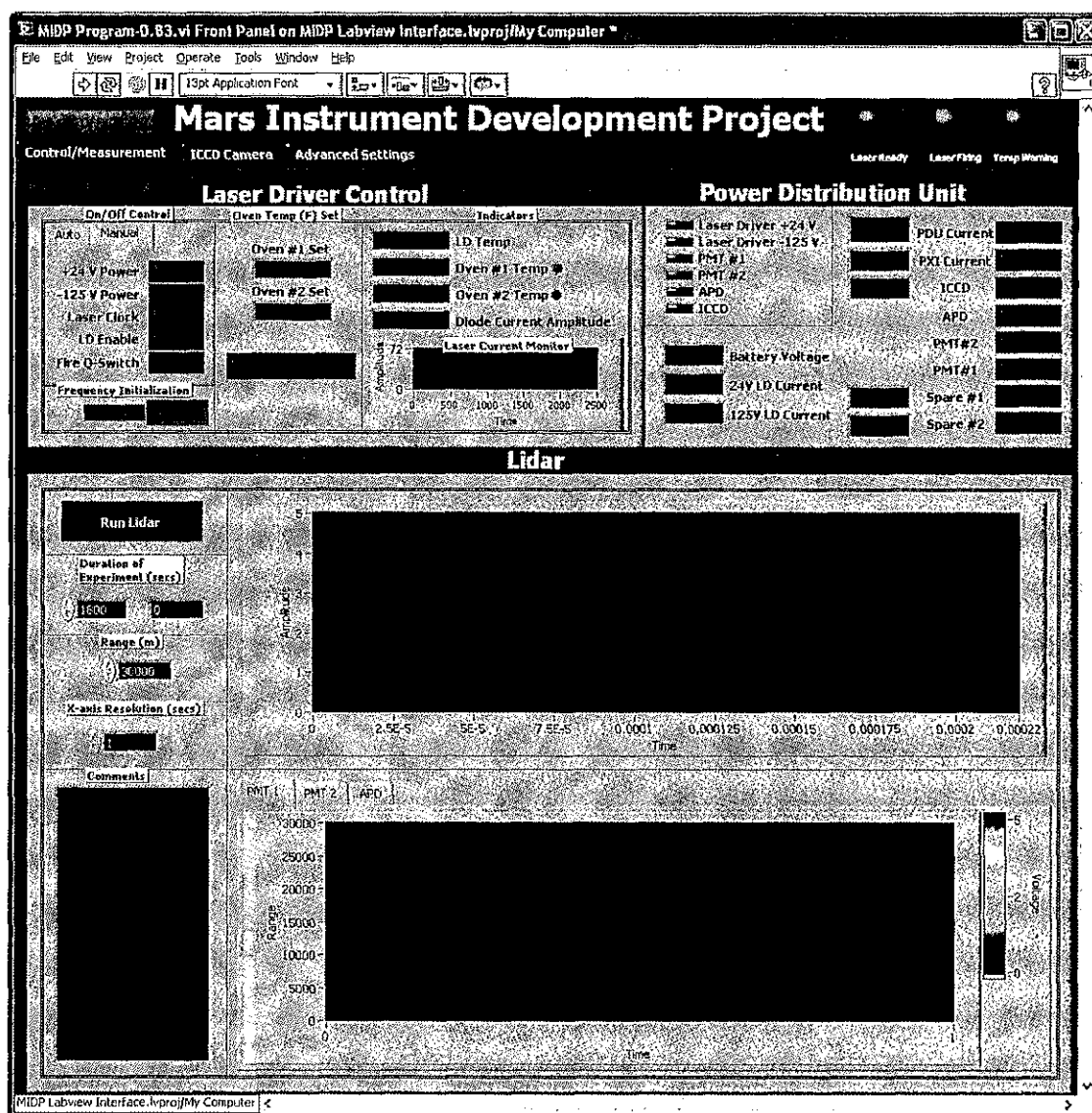
The LabVIEW program has a built in automatic power up setting that automatically turns on the laser and sets the oven temperatures. The control panel also contains various indicators such as laser diode current and battery voltage. The PXI chassis samples at a 10 MHz rate; therefore, we have a resolution of 15 meters. Since each shot is saved in a text file, the size of the text

file will depend on the desired range. For example, if the range was set to 150

meters, then there would be 10 rows of data in a saved shot text file. Therefore,

there is an option for Range to reduce file size (which is normally set to 10 km).

By clicking the "Run Lidar" button on the control panel, a lidar experiment will

begin and each laser shot text file is saved to an external hard drive connected to

the remote laptop. During the experiment, a live view of the lidar return signal can

be seen on the two display graphs.

All data analysis is also done on the remote laptop using MATLAB

software. Different files have been created to perform background correction and

range squared correction.

2.6 Lidar Experimental Setup

A diagram of the basic setup for the lidar experiment is shown in Figure

13, and a picture of the rover in lidar mode is given in Figure 14. The space-

qualifiable laser sends 20 Hz laser pulses into the atmosphere during a lidar

experiment. The 355 nm, 532 nm, and 1064 nm laser outputs are always

transmitted and give returns from the atmosphere, but this thesis is only

interested in the atmospheric aerosol and cloud returns from the 532 nm laser

output. The telescope collects the return pulses from the atmosphere and

focuses them into a 1 mm fiber optic cable, which is connected to the receiving

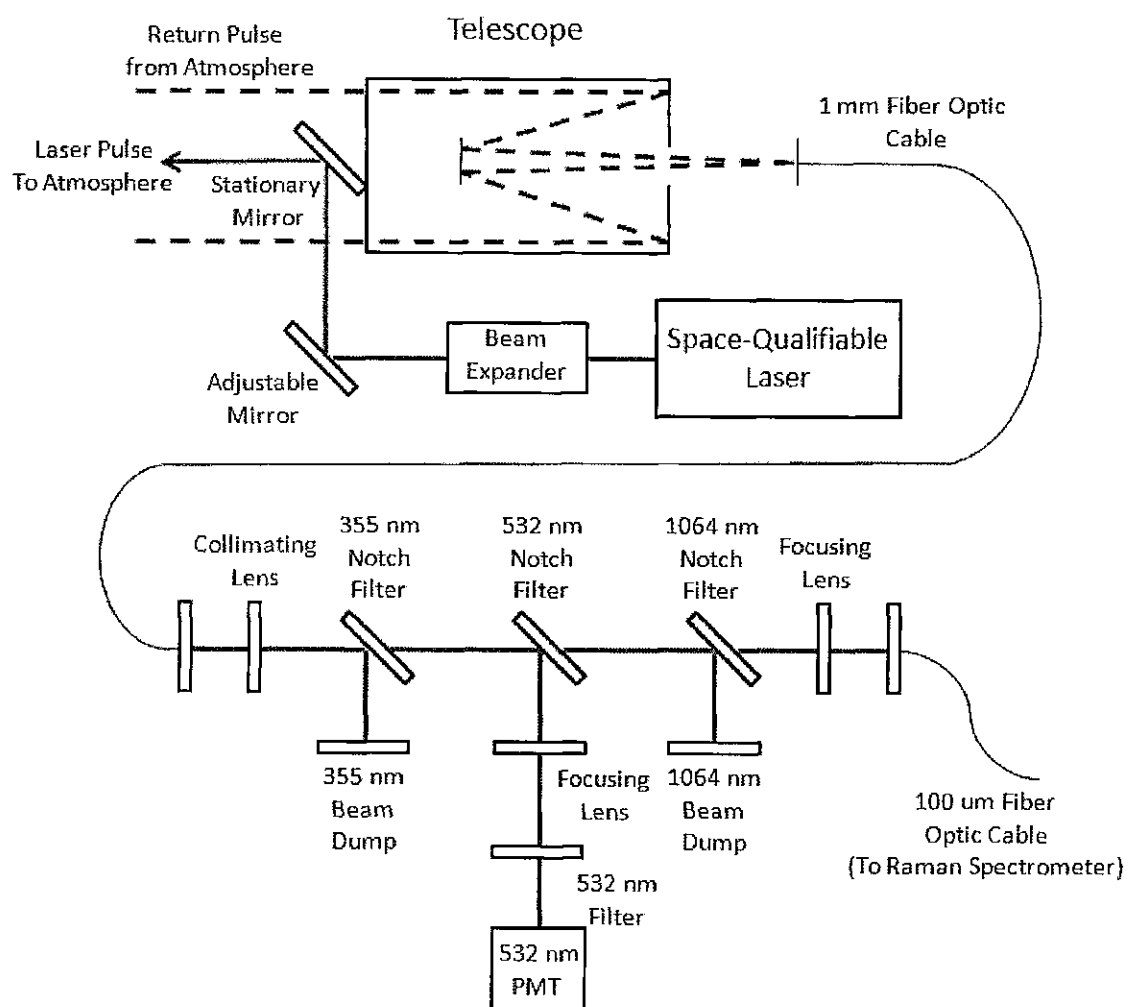optics. As part of the receiving optics, a PMT is used to detect the atmospheric return signals.

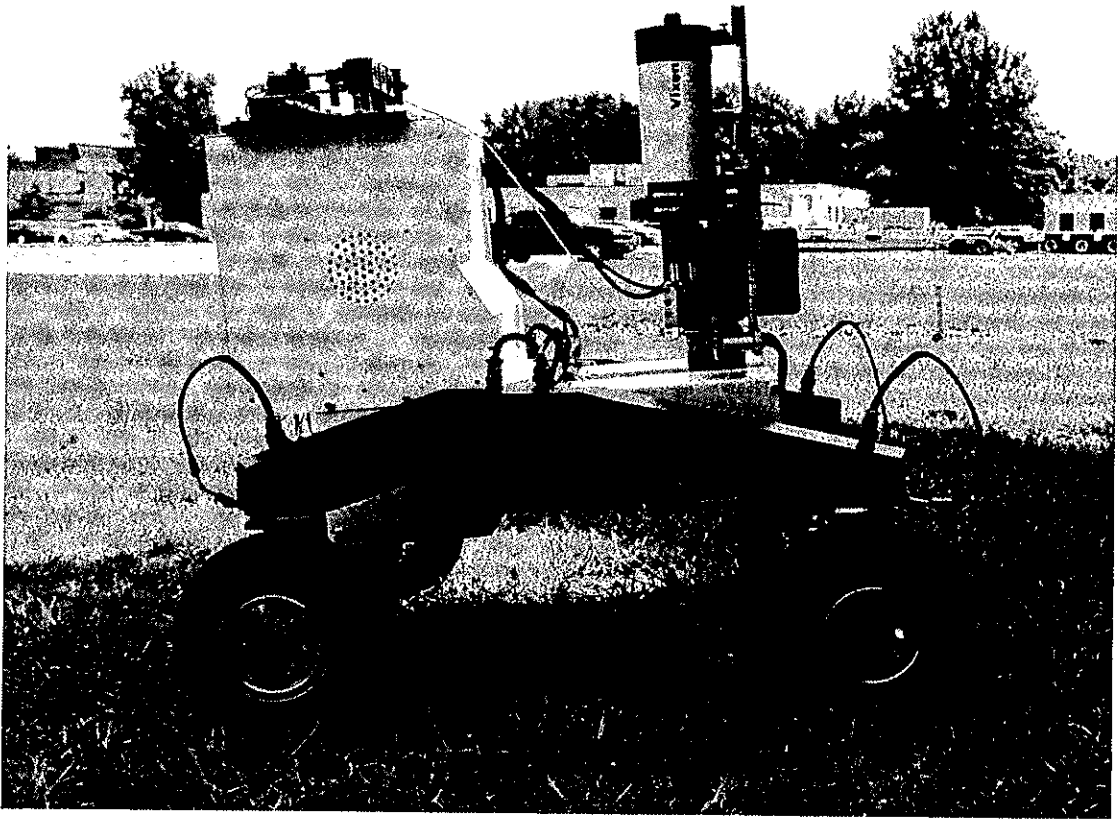Figure 13: Rover lidar setup for aerosol and cloud measurements.

Figure 14: Rover in lidar mode.

CHAPTER III

ROVER LIDAR SYSTEM RESULTS

In this chapter, a lidar simulation will be performed using the previously described lidar equation in equation (11). For this equation, the unknown variables are the backscatter coefficient β and the extinction coefficient α. Atmospheric effects by aerosols and molecules will be considered in theoretical calculations of the lidar return signal based on lidar system parameters used for this thesis. Lastly, the lidar system was used to perform atmospheric lidar measurements using the 532 nm aerosol channel, and the results are presented in the following sections.

3.1 Molecular Coefficients

As shown in equation (11), the molecular scattering coefficients are the molecular backscattering coefficient $\beta_{mol}(R)$ and the molecular extinction coefficient $\alpha_{mol}(R)$. These two molecular scattering properties can be determined either from the best available data of temperature and pressure or from standard atmospheric data so that only the aerosol coefficients are unknown. The molecular backscattering coefficient can be calculated theoretically by using the particle extinction-to-backscatter ratio, also known as the lidar ratio, which is given as[10]

$$\beta_{mol}(R) = \frac{3}{8\pi} \alpha_{mol}(R)$$.(12)

This still leaves three total unknowns for the lidar equation, and more equations will be needed in order to plot an expected lidar return signal. The molecular extinction coefficient can be approximated by considering extinction from gas molecules. Elastic scattering by gas molecules can be expressed using the Rayleigh scattering cross-section σ_R and the molecular extinction coefficient can be expressed as[15]

$$\alpha_{mol}(R) = N_{mol}(R)\sigma_R$$.(13)

The term $N_{mol}(R)$ is dependent on range, and it represents the molecular number density in m^{-3}. The Rayleigh scattering cross-section for a given wavelength at altitudes below 100 km is given by equation (14).[15]

$$\sigma_R = 4.56\left[\frac{0.55}{\lambda(\mu m)}\right]^4 x10^{-31} m^2$$ (14)

As a result, the theoretical equation that is used to calculate the molecular extinction coefficient is shown in equation (15).[16]

$$\alpha_{mol}(R) = N_{mol}(R)4.56\left[\frac{0.55}{\lambda(\mu m)}\right]^4 x10^{-31} m^{-1}$$ (15)

3.2 Aerosol Coefficients

As shown in equation (11), the aerosol scattering coefficients are the aerosol backscattering coefficient $\beta_{aer}(R)$ and the aerosol extinction coefficient $\alpha_{aer}(R)$. The aerosol extinction coefficient can be determined from available data sets based on the range R, but the backscattering coefficient must be calculated using equation (16).[16]

$$\beta_{aer}(R) = \frac{\alpha_{aer}(R)}{35} \tag{16}$$

3.3 Receiver Efficiency and Conversion Factor

The efficiency of the receiving optics was determined using an Oriel Model 66181 continuous white light source and an Oriel Model 77200 monochromator to produce a 532 nm beam of light. This green light was then focused into the 1 mm fiber optic cable that normally connects the telescope to the receiving optics. By using a power meter, the intensity of the transmitted light was measured at various points to determine the efficiency of the system. Initially light was measured at the output of the 1mm fiber optic cable and right before the 532 nm PMT (refer to Figure 11). The measured efficiency was found to be approximately 1.5%. This is poor efficiency, so further measurements were taken at the collimating lens, the 355 nm notch filter, the focusing lens, and the 532 narrowband pass filter. The results showed that the notch filters and the

narrowband pass filter were the reason for such poor efficiency. Each notch filter had an efficiency of approximately 50%, while the narrowband pass filter was only 10% efficient. Although the efficiency of the filter seems poor, it is necessary for the system since it protects the PMT from any possible near field high power reflections. The efficiency of the fiber optic cable was measured to be about 70%, the telescope efficiency was found to be approximately 90%, and the transmitter optics efficiency was found to be about 50%. The total efficiency of the system is defined as

$$Efficiency_{system} = (Efficiency_{telescope})(Efficiency_{fiber})(Efficiency_{rec.})(Efficiency_{trans.}) \quad .(17)$$

Using the values expressed in the previous paragraph, the total system efficiency was found to be approximately 0.5%.

The raw data recorded by the data acquisition system from the PMT is expressed in voltage, whereas the lidar equation in (11) is expressed in watts. Clearly, there was a need for a conversion factor in order to properly compare any measured results with theoretical results. In order to determine the conversion factor, the same light source and monochromator were set up as discussed in the beginning of this section. The 532 nm beam of light was sent to the receiving optics where it was focused onto the PMT. The gain of the PMT was set to -700 V for the applied voltage, and the intensity of the 532 nm light was measured using a power meter directly after the filter but before the PMT. The light measured before the PMT was approximately 56 μW, and the voltage

measured by the PMT was 1 V. Using these results, the conversion factor, which is defined as a ratio of volts to watts, was found to be 18 kV/W.

3.4 Theoretical Lidar Calculation

Using the general form of the lidar equation, which is shown again in equation (18), the theoretical lidar return signal for the rover lidar system was calculated.

$$P(R) = P_0[\beta_{aer}(R) + \beta_{mol}(R)]\frac{c\tau}{2}\frac{A}{R^2}\eta O(R)\exp\left\{-2\int_0^R[\alpha_{aer}(R') + \alpha_{mol}(R')]dR'\right\} \quad (18)$$

The backscatter and extinction coefficients were calculated based on the discussions in previous sections, and the remaining variables of the equation, which are unique for the lidar receiver system, are shown below in Table 1. The graphed result for the theoretical expected lidar return signal is displayed in Figure 15.

Table 1: Basic lidar equation values.

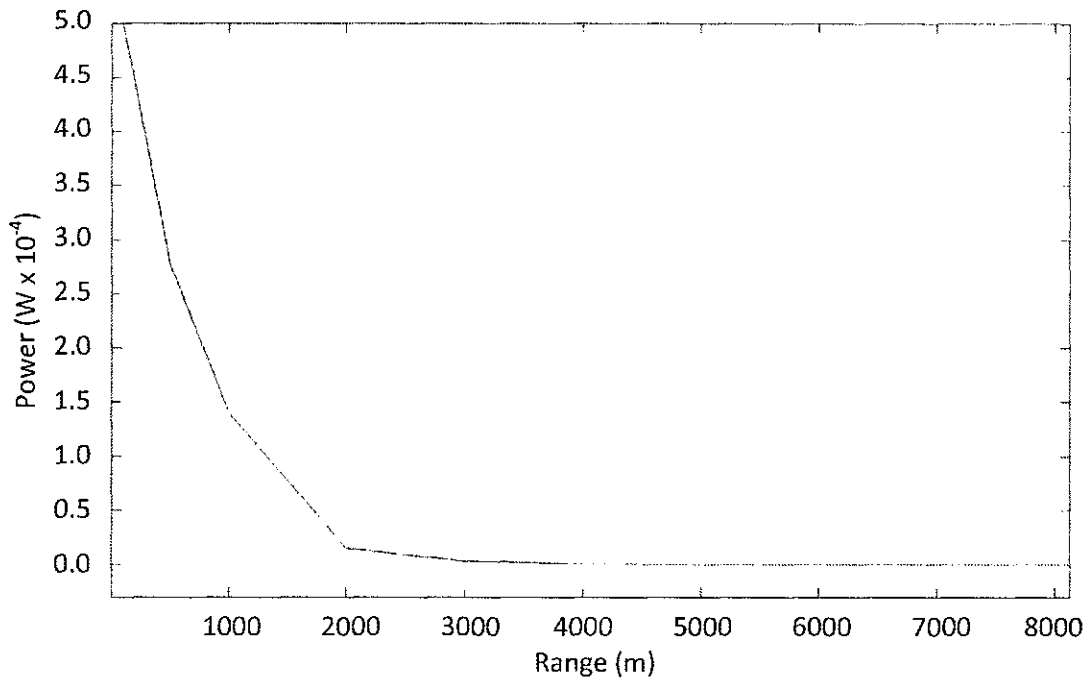| Lidar Parameter	Value
Power transmitted, P_0	1.25 MW
Effective spatial pulse length, $c\tau/2$	1.2 m
Telescope Area, A	0.009503 m^2
System Efficiency, η	0.005
Overlap, $O(R)$	1

Figure 15: Theoretical lidar return signal for rover lidar system.

3.5   532 nm Atmospheric Aerosol Tests

For the atmospheric tests, the 532 nm laser beam was transmitted into the atmosphere at a repetition rate of 20 Hz with a pulse energy of about 14 mJ. The first atmospheric test was performed on July 16, 2010 from approximately 12:00 PM to 1:00 PM. Figure 16 shows a plot of a raw single return signal, and Figure 17 illustrates the return signal intensity for the hour of testing. On this particular day, low-level clouds were visible in the sky, and a thin layer of clouds can be seen at approximately 1000 m on the intensity graph.

For data analysis, the data must be corrected for background noise and range. To determine the DC voltage offset created by atmospheric and system noise, the PMT is triggered to take data 200 µs before the laser is pulsed. This data is averaged for each shot and subtracted from the entire signal to account for noise correction. Since the lidar return signal decreases by $1/R^2$ as shown in equation (11), the range-corrected signal is defined by multiplying the raw return signal by R^2. Figures 18 and 19 show the background range-corrected lidar return signal and the background range-corrected return signal intensity, respectively. Noise subtraction can increase dramatically with the range-correction as seen in Figures 18 and 22.
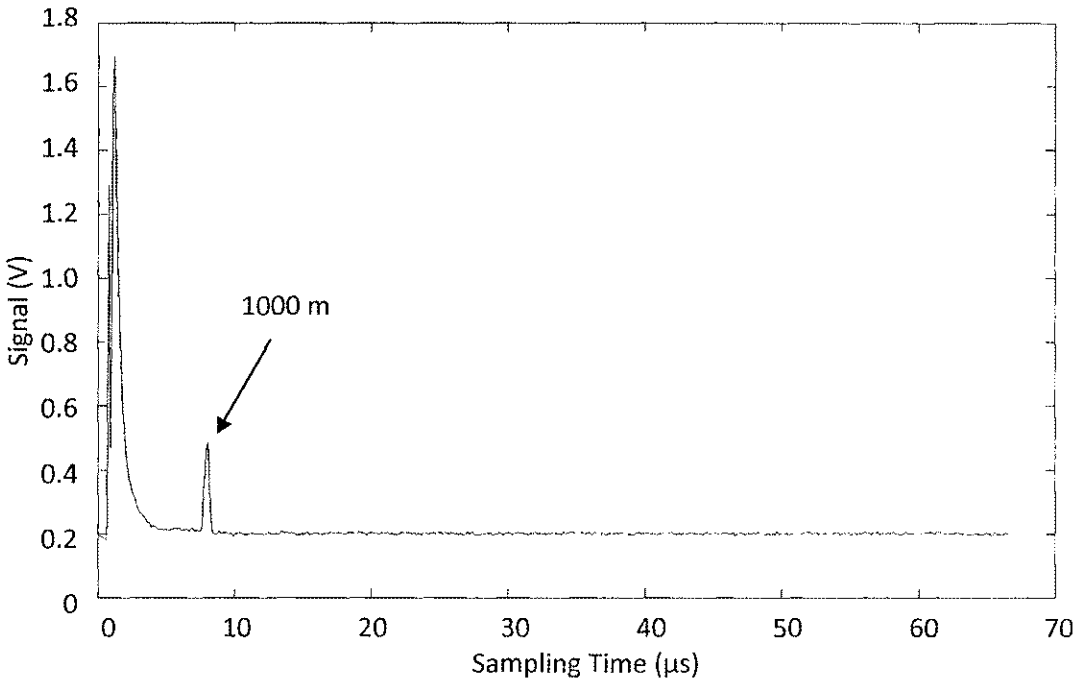

Figure 16: Raw lidar return signal on July 16, 2010.
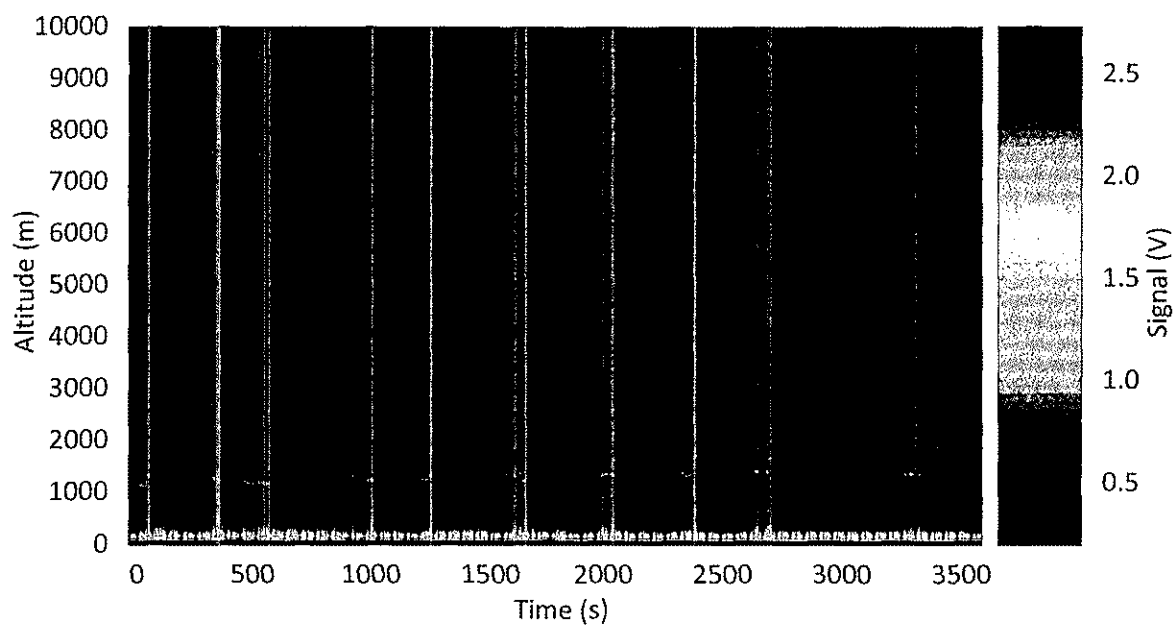
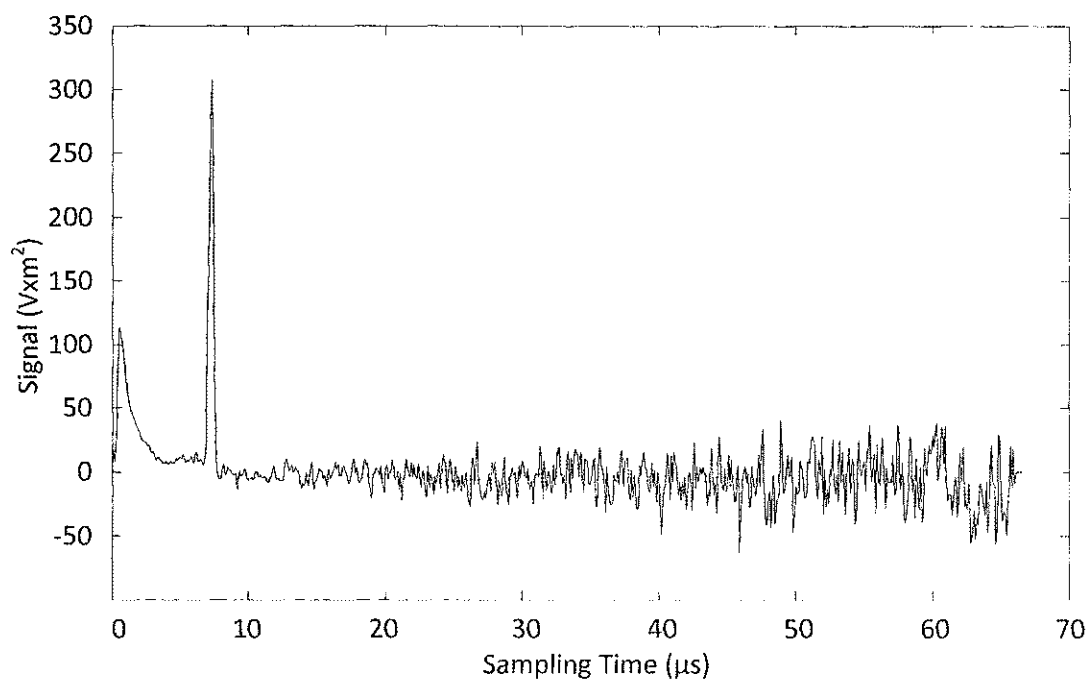Figure 17: Raw lidar signal image on July 16, 2010.

Figure 18: Background range-corrected lidar return signal on July 16, 2010.
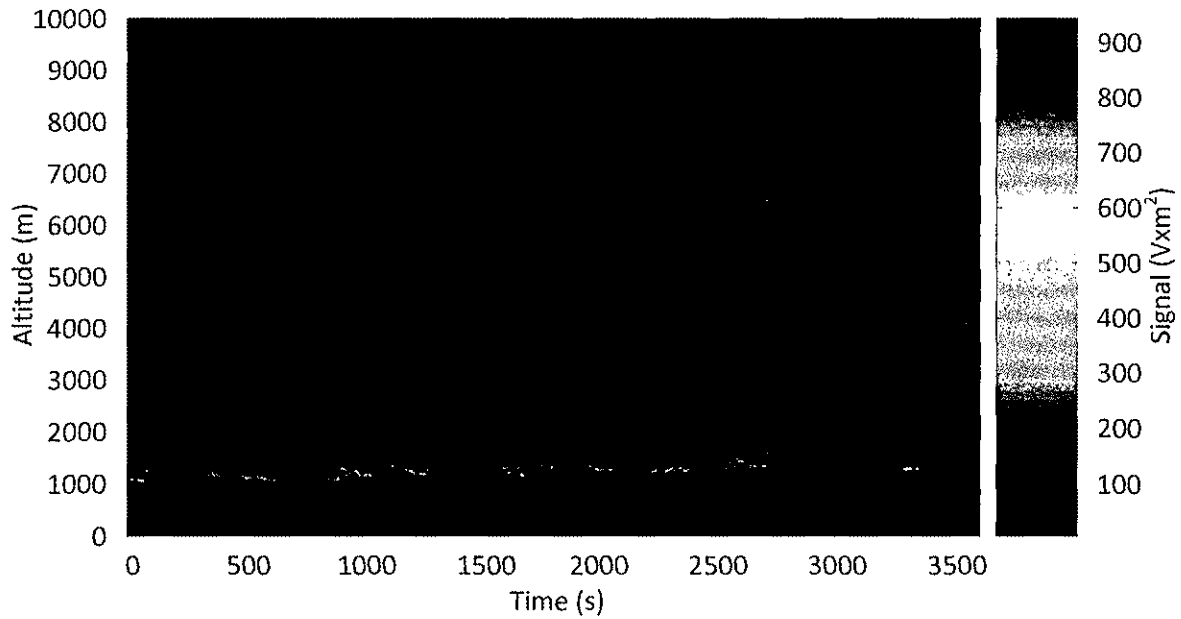
Figure 19: Background range-corrected lidar signal image on July 16, 2010.

The second atmospheric test was performed on August 20, 2010 from approximately 10:00 AM to 12:00 PM. This test was performed after minor modifications of the lidar receiver were made to improve the quality of the return signal. Figure 20 shows a plot of a raw single return signal, and Figure 21 illustrates the return signal intensity for the two hours of testing. Figures 22 and 23 show the background range-corrected lidar return signal and the background range-corrected return signal intensity, respectively. These two figures are 1 minute averages (1200 shot) as well. It was extremely humid and foggy on this particular day, so the boundary layer of the troposphere can easily be seen from 0 to 1500 m in Figure 23. Also, a thin cloud layer can be seen at approximately 2000 m, and a thin plume layer can be seen at approximately 2500 m.
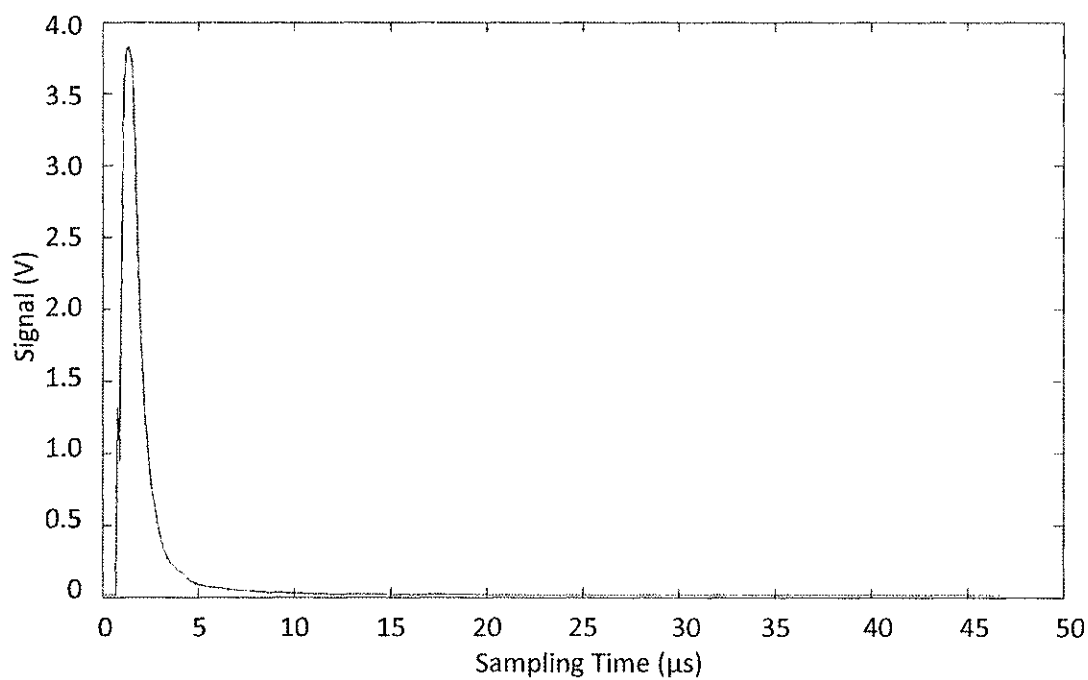
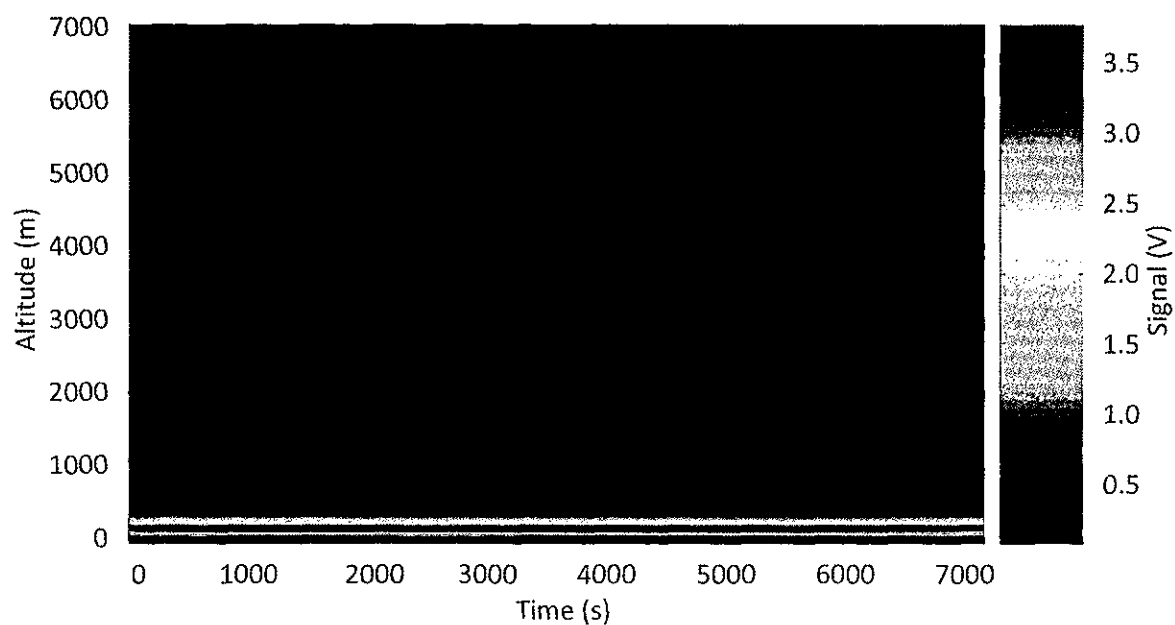Figure 20: Raw lidar return signal on August 20, 2010.

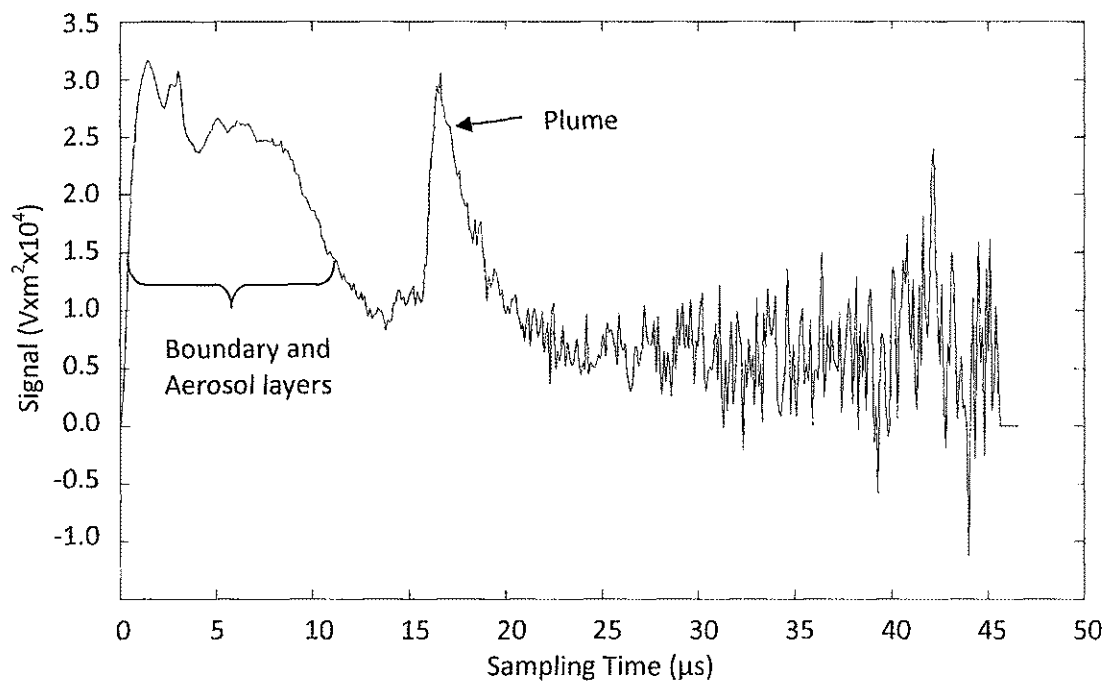Figure 21: Raw lidar signal image on August 20, 2010.

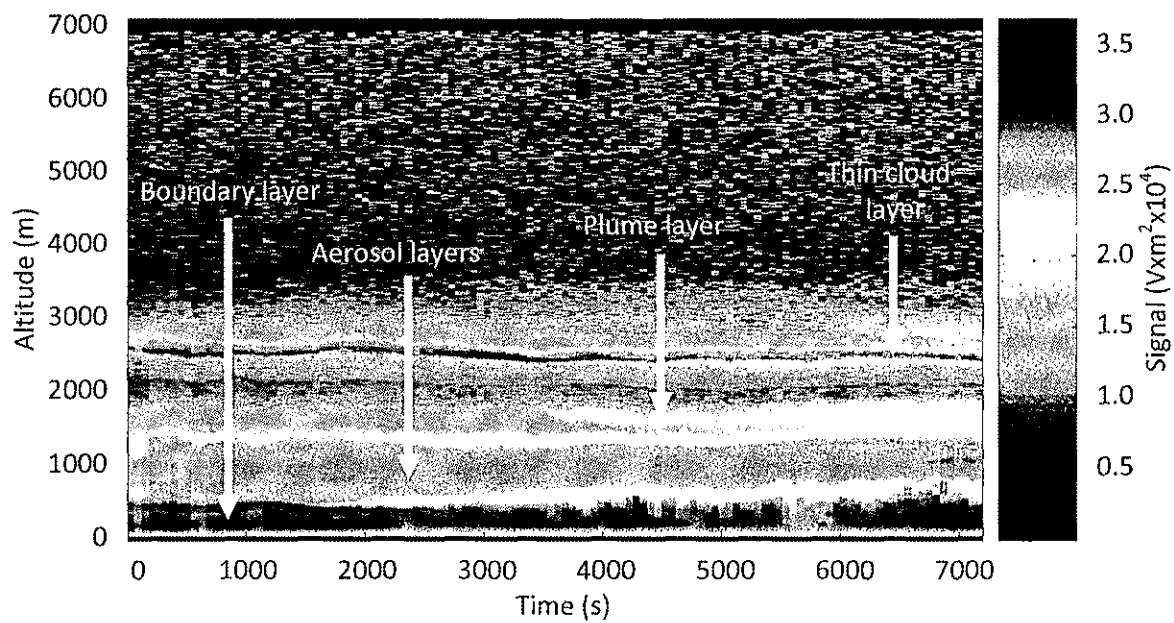Figure 22: Background range-corrected lidar return signal on August 20, 2010.

Figure 23: Background range-corrected lidar signal image on August 20, 2010.

CHAPTER IV

DISCUSSION

This chapter discusses the data obtained through the lidar receiver system and presents the atmospheric aerosol results. The various parameters used to calculate the theoretical lidar return signal are reviewed as well. In addition, the theoretical results are compared with the experimental results from the 532 nm atmospheric return signal. Finally, possible future work will be discussed in this section.

In order to test the lidar system, two experimental tests were conducted at separate times by transmitting the 532 nm laser beam to the atmosphere in order to detect scattered signals from clouds and aerosols. The backscattered light was collected by the telescope, passed through a 1 mm fiber optic cable, and was directed to the PMT through the receiving optics. The signal received by the PMT was then processed by the NI PXI data acquisition system and stored on an external hard drive connected to the remote computer used to control the rover lidar system. In the first test on July 16, 2010, relatively large temperature variations in the ovens were discovered that affected the energy in the outgoing laser beam. It was observed that the oven controllers were not wired properly, and corrective changes were made. A second test was performed on August 20, 2010. No problems arose during the second test, and the data that was collected proved to be an excellent set of data after analysis.

The conditions during the second atmospheric aerosol test on August 20, 2010 were extremely foggy and cloudy. Low-level clouds could easily be seen, and the lidar results that were obtained confirmed their presence in the sky. After analysis, the tropospheric boundary layer could be seen from 0 to 1500 m, and a thin cloud layer could be seen at 2500 m.

Theoretical calculations were carried out to compare with the measured results from the atmospheric test data. In order to compare the results, certain variables needed to be determined that were specific to the lidar system. The area of the telescope was known to be 0.009503 m^2 (100 mm diameter), and the transmitted power of the laser was known to be 1.25 MW. The overlap function, $O(R)$, was assumed to be 1 to allow for easier theoretical calculations. After power measurements, the system efficiency was found to be approximately 0.5%. The FWHM of the laser's 532 nm wavelength is 8 ns, and this number was used to determine the effective spatial pulse length. The theoretical lidar calculation considered both molecular and aerosol scattering, and their corresponding coefficients were determined. The molecular backscattering coefficient and the molecular extinction coefficient were determined using equations (12) and (15). The aerosol extinction coefficient was determined using available data, while the aerosol backscattering coefficient was calculated using equation (16). Table 2 provides a summary of the values used for the theoretical lidar equation variables.

Table 2: Summary of theoretical lidar variables with
backscatter and extinction coefficients.

Lidar Parameter	Value
Power transmitted, P_0	1.25 MW
Backscatter Coefficient, $\beta_{aer}(R)+\beta_{mol}(R)$	See Equations (12) and (16)
Effective spatial pulse length, $c\tau/2$	1.2 m
Telescope Area, A	0.009503 m^2
System Efficiency, η	0.005
Overlap, $O(R)$	1
Extinction Coefficient, $\alpha_{aer}(R)+\alpha_{mol}(R)$	See Equation (15)

In order to provide an accurate comparison between the theoretical and measured lidar signal, the area in front of the PMT was chosen as a point of reference. The PMT provides raw lidar return signal data in units of voltage, but the lidar equation is measured in units of watts, so a conversion factor was necessary for proper comparison. In section 3.3, the conversion factor used to convert the raw return data from units of voltage to power was found to be 18 kV/W.

Using all of the values discussed previously, the theoretical results of the lidar equation were determined and compared to the measured results of the transmitted 532 nm laser beam. Figure 24 shows a graph of the theoretical and measured lidar signal results from August 20, 2010. The results show good agreement, but the theoretical results were found to be slightly higher than the measured results. This is likely due to the use of standard atmosphere values for

some of the lidar equation variables. The comparison of the results shows that the lidar system is capable of properly measuring lidar returns and can be used for atmospheric analysis.
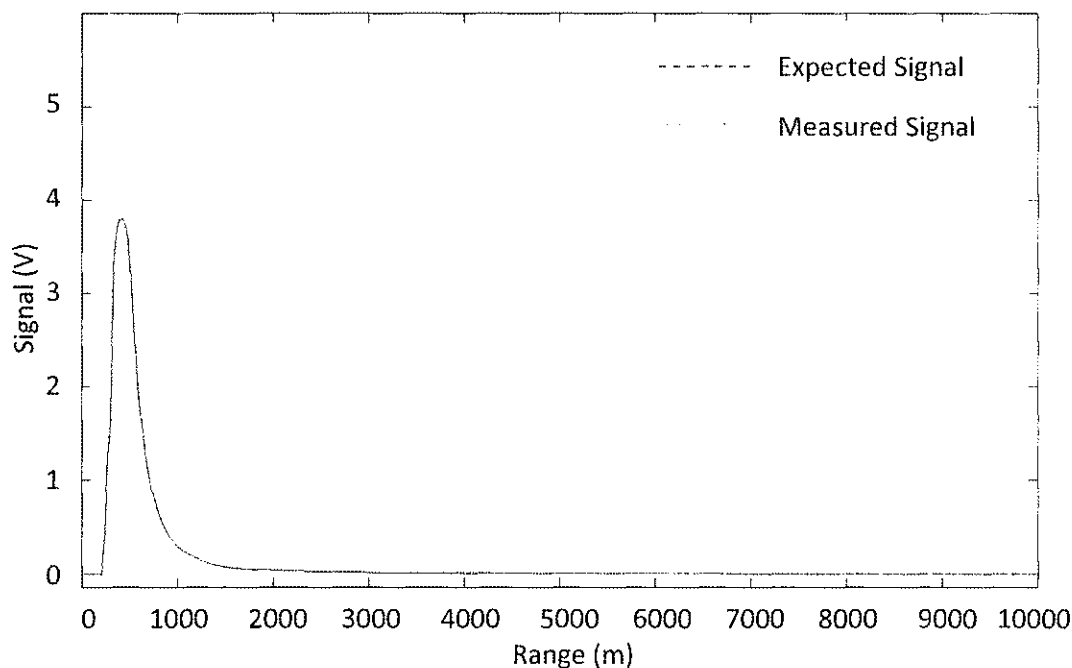

Figure 24: Comparison of theoretical and measured results.

Due to the nature of this work, future work can be done to provide better results and to increase the capabilities of the lidar rover system. The laser that is used, which is manufactured by Fibertek, is capable of providing three separate wavelengths of 355 nm, 532 nm, and 1064 nm. By adding another PMT or APD to the 355 nm and 1064 nm channels, more lidar return data could be obtained. By using data from all three wavelengths, ozone measurements and further data analysis could be performed. Also, the current notch filters have relatively poor

efficiency, so replacing them with more efficient filters may improve overall system efficiencies.

CHAPTER V

CONCLUSIONS

In this thesis, a compact rover lidar transmitter and receiver system for atmospheric aerosol measurements was designed and tested. The purpose and need for such a system was discussed, and all of the major subsystems (transmitter and receiver) were described in detail.

The 532 nm laser beam was transmitted to the atmosphere, and the backscattered signals were gathered by the lidar receiver system. The backscattered signal was directed to a PMT and voltage signals were received by a NI PXI data acquisition system that processed the data. The receiver and data acquisition system operated as expected.

Two atmospheric aerosol measurements were carried out on July 16, 2010 and August 20, 2010. Theoretical calculations of the lidar equation were determined based on the parameters of the rover lidar receiver system. These expected results showed good agreement with the measured results of the test on August 20, 2010. The measured results also showed excellent aerosol and plume distributions. As expected, the theoretical results were higher due to additional considerations of molecular scattering. The comparison showed that the rover lidar system was working properly and that it could be used to perform atmospheric aerosol lidar measurements.

The next step will require the addition of a PMT or APD to the 355 nm and 1064 nm receiver channels. This would give the rover lidar system the ability to measure ozone and aerosols. Future work could also include replacing the 3 existing notch filters with more efficient filters to provide better lidar return signals.

REFERENCES

1. J. H. Seinfeld and S. N. Pandis, *Atmospheric Chemistry and Physics – From Air Pollution to Climate Change*, John Wiley & Sons, Inc., New Jersey (2006).

2. CCSP 2009: *Atmospheric Aerosol Properties and Climate Impacts,* A Report by the U.S. Climate Change Science Program and the Subcommittee on Global Change Research. [Mian Chin, Ralph A. Kahn, and Stephen E. Schwartz (eds.)]. National Aeronautics and Space Administration, Washington, D.C., USA, 128 pp.

3. J. Reagan, M. McCormick, and J. Spinhirne, "Lidar Sensing of Aerosols and Clouds in the Troposphere and Stratosphere," *Proceedings of the IEEE* **77**(3), 433-448 (1989).

4. C. Billings, *Lasers, The New Technology of Light*, Oxford, New York (1992).

5. V. Kovalev and W. Eichinger, *Elastic Lidar*, John Wiley & Sons, Inc., New Jersey (2004).

6. T. Fujii and T. Fukuchi, *Laser Remote Sensing*, Taylor & Francis Group, LLC, Boca Raton (2005).

7. De La Salle University-Manila LIDAR Research Group, Basic Lidar Principle, http://mysite.dlsu.edu.ph/faculty/vallare/lidarsystem.html.

8. American Meteorological Society, Glossary of Meteorology, http://amsglossary.allenpress.com/glossary/search?p=1&query =lidar+equation.

9. P. K. Rastogi, *Optical Measurement Techniques and Applications*, Artech House, Inc., Norwood (1997).

10. C. Weitkamp, *Lidar*, Springer, New York (2005).

11. Leibniz Institute for Tropospheric Research, "Optical Remote Measurements – Analysis of Atmospheric Processes with Optical Methods," http://lidar.tropos.de/en/research/lidar.html.

12. Fibertek, Inc., *Compact Space-Based Laser Final Report*.

13. J. T. Verdeyen, *Laser Electronics*, Prentice Hall, Inc., New Jersey (2000).

14. R. Paschotta, "YAG Lasers", *Encyclopedia of Laser Physics and Technology*, http://www.rp-photonics.com/yag_lasers.html.

15. E. D. Hinkley, *Laser Monitoring of the Atmosphere*, Springer, New York (1976).

16. R. M. Measures, *Laser Remote Sensing*, John Wiley & Sons, Inc., New York (1984).

VITA

NAME: Benjamin D. Robinson
DATE OF BIRTH: August 9, 1987

DEGREES:

Master of Science (Electrical Engineering), Old Dominion University,
    Norfolk, Virginia, 2011
Bachelor of Science (Electrical Engineering), Old Dominion University,
    Norfolk, Virginia, 2009

EXPERIENCE:

NASA, Hampton, VA Masters Thesis Research	August 2009 – Present
NASA, Hampton, VA Lidar Senior Design Project	January 2009 – May 2009
SPAWAR Systems Center Atlantic Interior Voice Communications	August 2008 – Present

GRANTS AND CONTRACTS AWARDED:

Virginia Space Grant Consortium Graduate Fellowship

PROFESSIONAL SOCIETY MEMBERSHIP:

IEEE, Tau Beta Pi Honor Society, Phi Kappa Phi Honor Society